gene-specific quantized or possibly combinatorial assembly of sets of discrete protein complexes. The unique distribution of sites of RNA secondary structure for each nuclear RNA molecule might underlie the organization, although other factors like pauses in transcription might also contribute. In sum, monoparticles appear to be built from complex oligomeric protein interactions that serve to fold the RNA and, given the dynamic role of nRNPs, may have important implications for RNA processing and transport.

Received for publication 30 May 1985.

REFERENCES

1. Beyer, A. L., O. L. Miller, and S. L. McKnight. 1980. Ribonucleoprotein structure in nascent hnRNA is on-random and sequence-dependent. *Cell.* 26:155–165.
2. Beyer, A. L., M. E. Christensen, B. W. Walker, and W. M. LeStourgeon. 1977. Identification and characterization of the packaging proteins of core 40S hnRNP particles. *Cell.* 11:127–138.
3. Lothstein, L., H. P. Arenstorf, S.-Y. Chung, B. W. Walker, J. C. Wooley, and W. M. LeStourgeon. 1985. General organization of protein in HeLa 40S nuclear ribonucleoprotein particles. *J. Cell Biol.* 100:1570d–1581.
4. Mossesson, M. W., J. Hainfeld, R. H. Haschemeyer, and J. Wall. 1981. Identification and mass analysis of human fibrinogen molecules and their domains by STEM. *J. Mol. Biol.* 153:691–718.
5. Langmore, J., and J. Wooley. 1975. Chromatin architecture: investigation of a subunit of chromatin by dark field electron microscopy. *Proc. Natl. Acad. Sci. USA.* 72:2691–2695.
6. Wooley, J., and J. Langmore. 1977. Electron microscopic studies on nucleosome structure. *In* Molecular Human Cytogenetics. R. S. Sparkes, D. Comings, and F. Fox, editors. Academic Press, New York. 41–55.

BINDING OF ETHIDIUM TO BACTERIOPHAGES T7 AND P22

G. A. GREISS, P. SERWER, AND P. M. HOROWITZ,
Department of Biochemistry, The University of Texas Health Science Center, San Antonio, Texas 78284

Bacteriophages P22 and T7 are genetically unrelated, but each contains a linear molecule of double-stranded DNA packaged within a capsid of protein. The capsid consists of an outer shell of icosahedrally arranged subunits, a projection (tail) from the exterior of the shell, and internal proteins (reviewed in reference 1). The outer radius of the capsid is 30.1 nm for T7 (2) and 31.4 nm for P22 (3). In the case of T7, the internal proteins form a cylinder coaxial with the tail (4). An internal cylinder has not been observed in P22. To detect changes in the conformation of DNA that occur as a consequence of packaging in T7's capsid, equilibrium binding of ethidium to packaged T7 DNA was compared to equilibrium binding of ethidium to DNA released from the T7 capsid (free DNA) (5). It was found that 1.2% of the packaged nucleotide pairs formed high affinity sites with an enthalpy of binding more negative than the enthalpy of binding to either the majority of packaged DNA nucleotide pairs or the nucleotide pairs of free DNA. The high affinity sites were revealed by curvature in Scatchard (6) plots of ethidium binding to packaged DNA. The role of T7's internal cylinder in producing the high affinity sites is not known. In addition, no study of the kinetics of ethidium's binding to packaged DNA has been made for either T7 or P22. Here we describe a study of the equilibrium binding of ethidium to P22, and the rates of ethidium's entry into T7 and P22.

RESULTS AND DISCUSSION

To determine whether or not the internal cylinder of T7 is required for the high-affinity binding sites, equilibrium binding of ethidium to P22 was quantitated using a Scatchard plot. It was found that the curvature produced by T7's high-affinity sites at a molar ratio of ethidium/nucleotide pairs (r) below 0.02 was also present for P22 (Fig. 1). Thus, the T7 component(s) required for the high affinity sites are apparently also present in P22. Therefore,

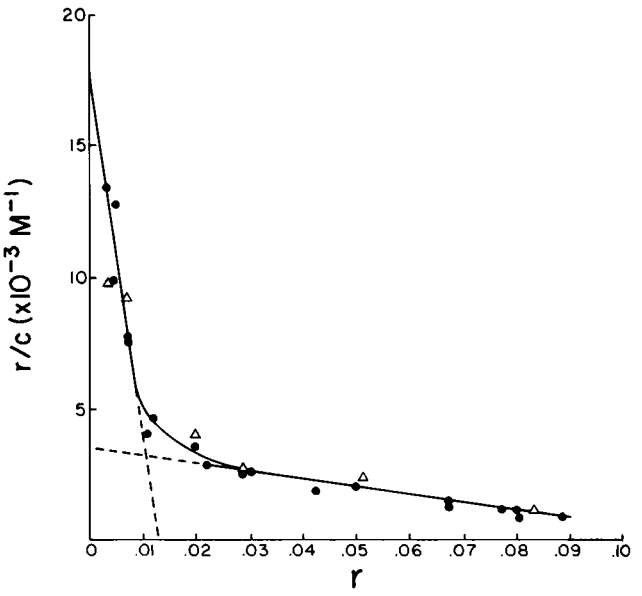

FIGURE 1 Binding isotherms for bacteriophages T7 and P22. Values of r/c at 25°C were plotted vs. r as previously described (6), where r is the molar ratio of bound ethidium to base pairs, and c is the concentration of unbound ethidium (●)-T7; (△)-P22.

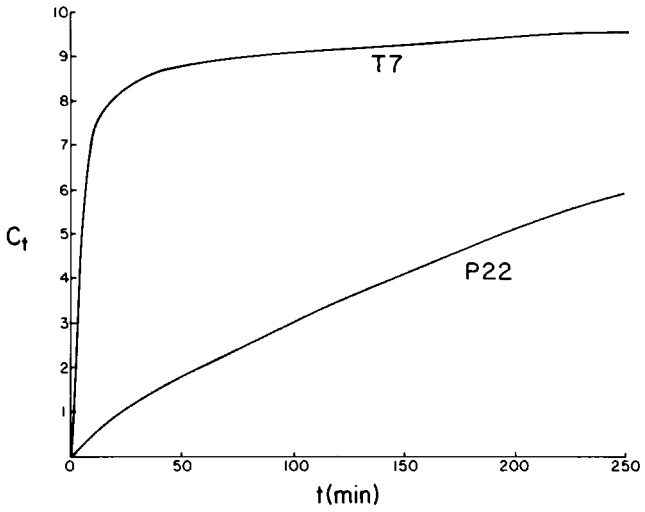

FIGURE 2 Kinetics of ethidium binding to T7 and P22 at 25°C. Fluorescence enhancement at 600 nm with 540 nm excitation: C_t in fluorescence units. Total ethidium concentration was 12.7 μM, and DNA base pair concentration was 60 μM.

T7's internal cylinder is not required for the high affinity sites.

In contrast to the similarity of binding isotherms for binding of ethidium to T7 and P22, the apparent rate of ethidium's binding was greater for T7 than P22. Values of ethidium bound per nucleotide pair at a given time, (C_t), were determined using fluorescence enhancement as previously described (5). A plot of C_t (Fig. 2) revealed the relatively slow binding to P22 DNA. If the kinetics are simple first order, then a semilogarithmic plot of the difference between C_t at equilibrium (C_e) and C_t is linear (7). Although this plot for T7 was linear at early times (Fig. 3), there was a decrease in slope at later times (concave curvature).

The curvature in Fig. 3 can be described using a model consisting of two first-order rate processes. For this model the rate constants (k_1, k_2) and equilibrium values of C_t (C_{e1}, C_{e2}) were determined by the procedure of Kezdy and Swinbourne (8). The parameters k_1 and C_{e1} were first determined from the early points. Then the calculated values of the contribution from the faster rate process were subtracted from the data points to generate a new data set with which to determine k_2 and C_{e2} by the same Kezdy-Swinbourne algorithm. When C_{e1} rather than C_e was used for T7 in the semilogarithmic plot in Fig. 3, a straight line was obtained (dashed line). A plot resulting from a similar analysis for the T7 slow phase was also linear (data not shown). Thus, an analysis in terms of two first-order phases describes the T7 data within experimental error. In contrast, the P22 data can be fitted with a single first-order phase, with the exception of the first 3% if dye bound. The P22 rate constant was 0.004 $^{-1}$, the same as T7's k_2 (0.004 min^{-1} and less than T7's k_1 (0.2 min^{-1}).

If passage of ethidium through a hole(s) in the capsid of

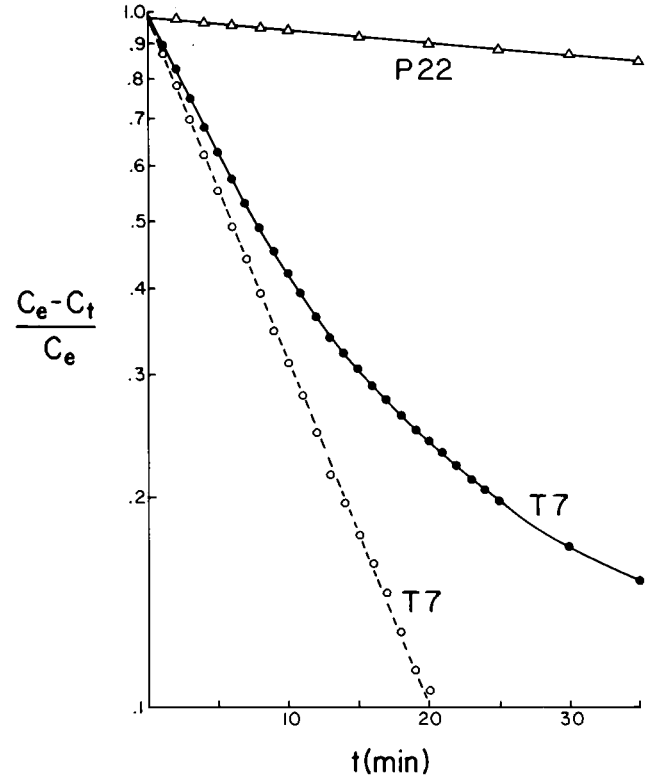

FIGURE 3 Test for first order reaction. After determination of C_e, C_{e1}, and C_{e2}, as described in the text, the normalized differences, $(C_e - C_t)/C_e$ were plotted semilogarithmically as a function of t (t_0 is the time of mixing). (-●-)-T7 using C_e; (-○-)-T7 using C_{e1}; (-△-)-P22 using C_e.

T7 and P22 were the rate-limiting step for binding, zero-order binding kinetics would be expected, i.e., the plots in Fig. 3 would have convex curvature. The data do not support this interpretation. Further investigations are being made of the possibility that passage through the DNA-containing region of the capsid's interior is the rate-limiting step.

Support was received from the National Institutes of Health, grant GM24365 to P. Serwer and GM25177 to P. M. Horowitz. The Robert A. Welch Foundation supported P. Serwer (grant AQ-764) and P. M. Horowitz (AQ-723).

Received for publication 30 April 1985.

REFERENCES

1. Earnshaw, W. C., and S. R. Casjens. 1980. DNA packaging by the double-stranded DNA bacteriophages. *Cell.* 21:319–331.
2. Stroud, R. M., P. Serwer, and M. J. Ross. 1981. Assembly of bacteriophage T7; dimensions of the bacteriophage and its capsids. *Biophys. J.* 36:743–757.
3. Earnshaw, W., S. Casjens, and S. C. Harrison. 1976. Assembly of the head of bacteriophage P22: X-ray diffraction from heads, proheads and related structures. *J. Mol. Biol.* 104:387–410.
4. Serwer, P. 1976. Internal proteins of bacteriophage T7. *J. Mol. Biol.* 107:271–291.

5. Griess, G. A., P Serwer, and P. M. Horowitz. 1985. Binding of ethidium to bacteriophage T7 and T7 deletion mutants. *Biopolymers*. In Press.
6. Scatchard, G. 1949. The attraction of proteins for small molecules and ions. *Ann. NY Acad. Sci.* 51:660–672.
7. McCall, P. J., and V. A. Bloomfield. 1976. Kinetics of proflavin binding to bacteriophages T2L and T4D. *Biopolymers*. 15:2323–2336.
8. Moore, J. W., and R. G. Pearson. 1981. Kinetics and Mechanism. John Wiley & Sons, Inc., New York.

STRUCTURAL STUDIES OF ADENOVIRUS TYPE 2 AND AN ASSEMBLY MUTANT

C. BERTHET-COLOMINAS,* P. BOULANGER,‡ C. DEVAUX,*‡ B. JACROT,* AND P. A. TIMMINS§
**European Molecular Biology Laboratory Grenoble Outstation, c/o Institut Laue-Langevin, 38042 Grenoble Cedex, France; ‡Laboratoire de Virologie, Institut National de la Santé et de la Récherche Medicale, 59045 Lille, France; and §Institut Laue-Langevin, 38042 Grenoble Cedex, France*

Adenovirus type 2 is an icosahedral mammalian virus containing 22.2 × 10^6 d of genomic DNA and some 10 structural proteins having a total molecular mass ~140 × 10^6. The structure of the major coat protein, the hexon, representing some 65% of the total protein, has been solved to 2.9 Å resolution by Burnett and colleagues (1). High-resolution studies are also being carried out on the fiber protein that attaches to the fivefold apices of the virus (2). Here we describe experiments using x-ray and neutron diffraction, electron microscopy with image reconstruction, and biochemical techniques aimed at investigating various aspects of the organization of adenovirus 2. In addition to native virus we have investigated a temperature-sensitive mutant H_2ts112 which, when grown at the nonpermissive temperature, contains only a small piece of DNA and lacks at least one major protein. We have also studied groups of nine hexons (GON) which are whole facets of the viral icosahedron obtained by treating the particle with sodium deoxycholate (3).

MATERIALS AND METHODS

Viral particles were grown in KB cells at 37°C for 40 h (human adenovirus type 2 wild type) or at the nonpermissive temperature, 38.5°C, for 20 h (mutant H_2ts112). Purification and isolation of viral particles and GON was achieved as described previously (4). Neutron scattering measurements were carried out at the D11 small-angle scattering instrument of the Institut Laue-Langevin. Sample-detector distances of 2–20 m and incident neutron wavelengths of 5 and 10 Å were used. Sample concentrations were 0.2–2.0 mg/ml. X-ray scattering experiments were performed using a double focusing system on an Elliot GX13 rotating anode tube. Specimen-to-film distance was 100 mm. Electron microscopy in amorphous ice (5) was carried out using the Phillips EM400 at European Molecular Biology Laboratory, Heidelberg.

RESULTS

Small-angle neutron scattering data were measured from solutions of native Ad2 and the mutant dialyzed against the same buffer made up in 0%, 25%, 70% and 100% D_2O/H_2O mixtures. These scattering curves were fitted by spherical shell models (Fig. 1) as previously described for the native structure (4). The intensity at zero scattering angle yields a molecular weight of 157 × 10^6 for the native particle and 125 × 10^6 for the mutant. Using these values, the molecular weights of protein and DNA can be derived for the individual shells as shown in Table I. The radial organization of native and mutant viruses shows the latter to be a much more hollow particle encapsidating only about one fifth of the normal mass of DNA. The protein distribution is somewhat surprising: the mutant contains some 16 × 10^6 of protein in the core although it lacks the major core protein VII. This can be explained only by assuming that the immature precursor protein pVI is in the core and has not been inserted in the capsid. Similarly, the

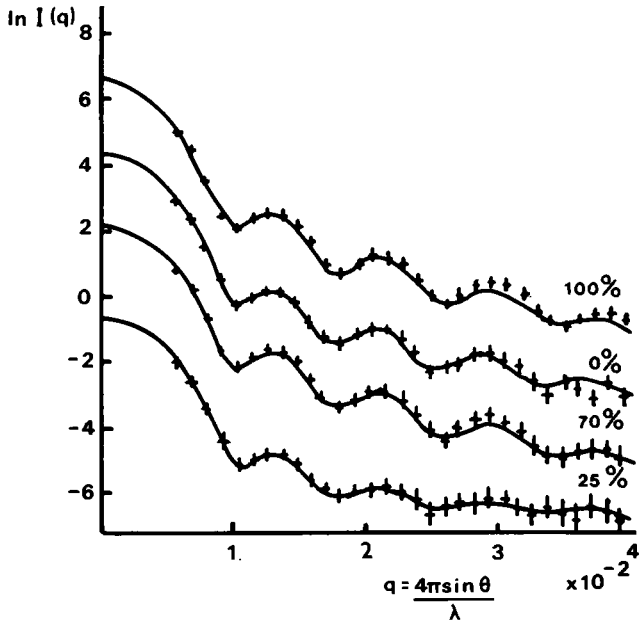

FIGURE 1 Small-angle neutron scattering curves from solutions of the adenovirus type 2 mutant H_2ts112 in various H_2O/D_2O mixtures. The dotted lines represent the experimental data and solid lines the fits of the model described in the table.